This article has been accepted for publication in a future issue of this journal, but has not been fully edited. Content may change prior to final publication. Citation information: DOI 10.1109/TCSII.2019.2915384, IEEE Transactions on Circuits and Systems II: Express Briefs

Auto-Tuning Proportional-Type Synchronization Algorithm for DC Motor Speed Control Applications

Chae Rin Lee, Seok-Kyoon Kim, and Choon Ki Ahn, *Senior Member, IEEE*

***Abstract*—This paper proposes an auto-tuning proportional-type synchronization controller for DC motor speed applications with consideration of parameter and load variations. The proposed algorithm is comprised of two parts: a proportional-type speed tracking controller with a disturbance observer (DOB) and second a synchronizer driven by an auto-tuning algorithm. The first feature is to propose an auto-tuning synchronizer to reduce synchronization error during transient operations. The second is to introduce a DOB so that the proportional-type controller guarantees tracking and synchronization performance recovery without offset error. Experimental experimental data is provided to convincingly show the effectiveness of the suggested scheme using a 50-W dual DC motor drive system.**

***Index Terms*—DC Motor, Speed synchronization, Auto-tuner, Disturbance observer**

I. Introduction

DC motors have been adopted for a wide range of applications, such as mobile robots, drones, 3D-printers, and manufacturing machines. Improved power efficiency and the capability to improve control performance are the main merits of DC motors. It has been reported that an advanced control algorithm can effectively enhance closed-loop control accuracy and performance [1]–[5].

In many applications, DC motor speed is adjusted via a cascade controller comprising a current- (inner) and speed-loop (outer) [6]. Each-loop can be controlled using a simple proportional-integral (PI) controller with well-tuned feedback gains by menas of several techniques, such as trial-error, loop-shaping, Bode, and Nyquist [7], [8]. The speed control performance can be improved by the application of various novel techniques used with three-phase induction and permanent magnet synchronous machines, such as robust, adaptive, neural network, feedback-linearization, sliding mode, model predictive, and disturbance-observer (DOB) based controllers. This is due to the similarity between DC motor and three-phase machine dynamics in the rotational d-q frame [9]–[19].

These methods can only establish the synchronization objective for speed regulation applications in the steady-state. They are insufficient, however, for industrial synchronization applications, like rolling mills and distributed paper manufacturing machines. There are preferred techniques, called cross-coupling and electronic shafting, to reduce the synchronization error using adjustable design parameters that act as an additive compensator to the speed controller [20], [21]. Parallel-type cross-coupling control was classically used by sharing each motor's speed information [22]. The relative cross-coupling technique, whose parameters must be calculated by solving matrix equations for each control period when the number of machines is greater than 2, was devised for a better performance [23], [24]. The sliding mode cross-coupling controller successfully cleared this practical limitation by proper modification of q-axis current reference signals using the synchronization errors of each motor [20]. Nonetheless, the motor parameter dependency problem still exists, and is the main motivation of this study.

This paper offers an advanced proportional-type controller accomplishing both the speed synchronization and the tracking tasks. The parameter and load variation problems are explicitly handled by introducing a perturbed dynamic model with DC machine nominal parameter values. The contributions are summarized as follows: a) an auto-tuning synchronizer updates the feedback gain to accelerate the synchronization error decay ratio in transient periods, and b) the introduction of a DOB enables the proportional-type controller to achieve beneficial closed-loop properties, namely, synchronization and tracking performance recovery and offset-free control. The merits of the proposed technique are experimentally confirmed using a dual 50-W DC motor control system.

II. Electrical and Mechanical Behavior of DC Motors

The application of Kirchhoff and Newton's second laws to the stator and rotor of the i-th DC motor leads to the set of differential equations:

$$J_i\dot{\omega}_i = -B_i\omega_i + k_{T,i}i_{a,i} - T_{L,i}, \quad (1)$$
$$L_{a,i}\dot{i}_{a,i} = -R_{a,i}i_{a,i} - k_{e,i}\omega + v_{a,i}, \quad (2)$$

$i = 1, 2, \cdots, N$, $\forall t \geq 0$ with the state variables of rotor mechanical speed ω_i (rad/s) armature current $i_{a,i}$ (A), and

This research was supported by Basic Science Research Program through the National Research Foundation of Korea (NRF) funded by the Ministry of Education (2018R1A6A1A03026005) and in part by the NRF of Korea through the Ministry of Science, ICT and Future Planning under Grant NRF-2017R1A1A1A05001325.

(Corresponding Author: Seok-Kyoon Kim and Choon Ki Ahn)

Chae Rin Lee is with the Graduate School of Creative Convergence Engineering, Hanbat National University, Daejeon, 341-58, Korea. Email: doflscofls@gmail.com

Seok-Kyoon Kim is with the Department of Creative Convergence Engineering, Hanbat National University, Daejeon, 341-58, Korea. Email: lotus45kr@gmail.com

Choon Ki Ahn is with the School of Electrical Engineering, Korea University, Seoul, 136-701, Korea. Email: hironaka@korea.ac.kr

This article has been accepted for publication in a future issue of this journal, but has not been fully edited. Content may change prior to final publication. Citation information: DOI 10.1109/TCSII.2019.2915384, IEEE Transactions on Circuits and Systems II: Express Briefs

the armature voltage $v_{a,i}$ (V) to be designed later. The load torque, denoted as $T_{L,i}$, acts as the mismatched external disturbances coming from the load conditions. The mechanical and electrical machine parameters are given as follows: J_i : moment inertia, B_i : viscous damping, $k_{T,i}$: torque constant, $L_{a,i}$: armature inductance, $R_{a,i}$: armature resistance, $k_{e,i}$: back EMF constant.

Load conditions can cause variations of DC motor parameters and load torque that must be taken into account to ensure consistent closed-loop performance for a wide operating range. To this end, rewrite the DC motor model of (1)-(2) using the nominal parameter values of $J_{0,i}$, $B_{0,i}$, $k_{T0,i}$, $L_{a0,i}$, $R_{a0,i}$, and $k_{e0,i}$ as

$$J_{0,i}\dot{\omega}_i = -B_{0,i}\omega_i + k_{T0,i}i_{a,i} + d_{\omega,i}, \quad (3)$$

$$L_{a0,i}\dot{i}_{a,i} = -R_{a0,i}i_{a,i} - k_{e0,i}\omega + v_{a,i} + d_{i_a,i}, \quad (4)$$

$i = 1, 2, \cdots, N$, $\forall t \geq 0$, with the unknown time-varying lumped disturbances of $d_{\omega,i}$ and $d_{i_a,i}$, which are used as the basis for controller design in the next section with the feedback signals of ω_i and $i_{a,i}$. It can be seen that the previous DOB-based results are developed under similar system model modifications [19].

III. SYNCHRONIZATION CONTROLLER DESIGN

The control task of this section is into two parts: a) the tracking task of $\lim_{t\to\infty}\omega_i = \omega_{ref}$, $i = 1, \cdots, N$, with ω_{ref} being the speed reference; b) the synchronization task of $\lim_{t\to\infty}\Delta\omega_i = \Delta\omega_{i,ref}$, $i = 1, \cdots, N-1$, with $\Delta\omega_i := \omega_i - \omega_{i+1}$ (synchronization error), and $\Delta\omega_{i,ref} = 0$, $\forall t \geq 0$. Moreover, this study introduces the desired control performance:

$$\frac{\Omega_i(s)}{\Omega_{ref}(s)} = \frac{\Delta\Omega_i(s)}{\Delta\Omega_{i,ref}(s)} = \frac{\omega_{sc}}{s + \omega_{sc}}, \ \forall s \in \mathbb{C}, \quad (5)$$

for a cut-off frequency of ω_{sc} (rad/s), where $\mathcal{L}\{\omega_{ref}(t)\} = \Omega_{ref}(s)$, $\mathcal{L}\{\omega_i(t)\} = \Omega_i(s)$, $\mathcal{L}\{\Delta\omega_{i,ref}(t)\} = \Delta\Omega_{i,ref}(s)$, and $\mathcal{L}\{\Delta\omega_i(t)\} = \Delta\Omega_i(s)$ with $\mathcal{L}\{(\cdot)\}$ representing the Laplace transform operator.

A. Control Algorithm

Before designing the controller, it is necessary to simplify the relationship from the control input of $v_{a,i}$ to the DC motor speed of ω_i. The armature current dynamics of (4) can be written as $i_{a,i} = -\frac{k_{e0,i}}{R_{a0,i}}\omega + \frac{1}{R_{a,0}}v_{a,i} + \frac{1}{R_{a,0}}d_{i_a,i} - \frac{L_{a,0}}{R_{a,0}}\dot{i}_{a,i}$, $i = 1, \cdots, N$, $\forall t \geq 0$, which results in the first-order input-output relationship between the armature voltage and the motor speed:

$$\frac{J_{0,i}R_{a0,i}}{k_{T0,i}}\dot{\omega}_i = v_{a,i} + d_i, \ i = 1, \cdots, N, \ \forall t \geq 0, \quad (6)$$

with a lumped disturbance of $d_i := -\frac{J_{0,i}R_{a0,i}}{k_{T0,i}}(B_{0,i} + \frac{k_{T0,i}k_{e0,i}}{R_{a0,i}})\omega_i + \frac{k_{T0,i}}{R_{a,0}}d_{i_a,i} - \frac{J_{0,i}L_{a,0}}{k_{T0,i}}\dot{i}_{a,i} + d_{\omega,i}$, $i = 1, \cdots, N$, $\forall t \geq 0$. This simplification can make the controller cost low by the elimination of the armature current feedback loop.

The controller is proposed for the DC motor dynamics of (6) to be stabilized as

$$v_{a,i} = \frac{J_{0,i}R_{a0,i}}{k_{T0,i}}\hat{\omega}_{sc}\tilde{\omega}_i - \hat{d}_i, \ i = 1, \cdots, N, \ \forall t \geq 0, \quad (7)$$

with the speed tracking error of $\tilde{\omega}_i := \omega_{ref} - \omega_i$, $\forall t \geq 0$, where the feedback gain of $\hat{\omega}_{sc}$ is adjusted by the auto-tuning synchronizer:

$$\dot{\hat{\omega}}_{sc} = \gamma_{at}\left(\sum_{i=1}^{N-1}\Delta\omega_i^2 + \rho_{at}\tilde{\omega}_{sc}\right), \ \forall t \geq 0, \quad (8)$$

with $\gamma_{at} > 0$ and $\rho_{at} > 0$ as tuning parameters. This shows that the synchronization error of $\Delta\omega_i$ excites the feedback gain, and the error damping term of $\tilde{\omega}_{sc} := \hat{\omega}_{sc}(0) - \hat{\omega}_{sc}$ with $\hat{\omega}_{sc}(0) = \omega_{sc}$ stabilizes the feedback gain dynamics. The disturbance estimate of $\hat{d}_i$ is obtained by the DOB:

$$\hat{d}_i = z_i + l_i\frac{J_{0,i}R_{a0,i}}{k_{T0,i}}\omega_i, \quad (9)$$

$$\dot{z}_i = -l_iz_i - l_i^2\frac{J_{0,i}R_{a0,i}}{k_{T0,i}}\omega_i - l_iv_{a,i}, \ \forall t \geq 0, \quad (10)$$

with design parameter of $l_i > 0$, $i = 1, \cdots, N$.

In summary, the proposed synchronization controller can be implemented using the state voltage command of (7), auto-tuning synchronizer of (8), and DOB of (9)-(10) and with adjustable design parameters of ω_{sc}, γ_{at}, ρ_{at}, and l_i. Fig. 1 depicts the whole control system structure.

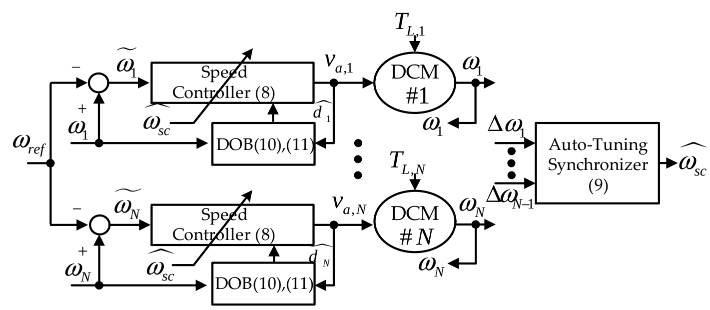

Fig. 1. Control system structure

B. Analysis

This section analyzes the closed-loop properties. First, the feedback gain lower bound of $\hat{\omega}_{sc}$ is established by Lemma 1.

Lemma 1: The feedback gain of $\hat{\omega}_{sc}$ driven by the proposed auto-tuning synchronizer of (8) is bounded below by its initial value of $\hat{\omega}_{sc}(0) = \omega_{sc}$, i.e., $\hat{\omega}_{sc} \geq \omega_{sc}$, $\forall t \geq 0$. ◊

Proof: The synchronizer of (8) corresponds to a linear time invariant (LTI) system as $\dot{\hat{\omega}}_{sc} = -\gamma_{at}\rho_{at}\hat{\omega}_{sc} + \gamma_{at}\rho_{at}\omega_{sc} + \gamma_{at}\sum_{i=1}^{n-1}\Delta\omega_i^2$ with the solution of $\hat{\omega}_{sc} = e^{-\gamma_{at}\rho_{at}t}\omega_{sc} + \int_0^t e^{-\gamma_{at}\rho_{at}(t-\tau)}(\gamma_{at}\rho_{at}\omega_{sc} + \gamma_{at}\sum_{i=1}^{n-1}\Delta\omega_i^2)d\tau \geq \omega_{sc}$, $\forall t \geq 0$, which completes the proof. ■

Now, consider the closed-loop error dynamics obtained by the substitution of (7) into (6) as

$$\dot{\omega}_i = \hat{\omega}_{sc}\tilde{\omega}_i + \frac{k_{T0,i}}{J_{0,i}R_{a0,i}}\tilde{d}_i, \ \forall t \geq 0, \quad (11)$$

This article has been accepted for publication in a future issue of this journal, but has not been fully edited. Content may change prior to final publication. Citation information: DOI 10.1109/TCSII.2019.2915384, IEEE Transactions on Circuits and Systems II: Express Briefs

with $\tilde{d}_i := d_i - \hat{d}_i$, $i = 1, \cdots, N$, $\forall t \geq 0$, which is utilized to achieve the convergence and tracking performance recovery properties in the following theorems.

Theorem 1: The proposed control scheme of (7) with auto-tuning synchronizer of (8) and DOB of (9)-(10) guarantees that $\lim_{t\to\infty} |\omega_i(t) - \omega_{ref}(t)| = 0$ as $\dot{\omega}_{ref}(t) \to 0$ and $\dot{d}_i(t) \to 0$, exponentially. $\diamondsuit$

Proof: The DOB output of (9) can be written as $z_i = \hat{d}_i - l_i \frac{J_{0,i} R_{a0,i}}{k_{T0,i}} \omega_i$, $\forall t \geq 0$, which turns the DOB dynamics of (10) into

$$\dot{\hat{d}}_i = l_i\left(\frac{J_{0,i} R_{a0,i}}{k_{T0,i}} \dot{\omega}_i - v_{a,i} - \hat{d}_i\right) = l_i(d_i - \hat{d}_i) = l_i \tilde{d}_i, \quad (12)$$

$\forall t \geq 0$, where the relationship of (6) is used to the second equality. Now, define the positive-definite function as

$$V_i := \frac{1}{2}\tilde{\omega}_i + \frac{\kappa_i}{2}\tilde{d}_i^2, \ i = 1, \cdots, N, \ \kappa > 0, \ \forall t \geq 0, \quad (13)$$

which satisfies that (using (11) and (12)): $\dot{V}_i = \tilde{\omega}_i(-\hat{\omega}_{sc}\tilde{\omega}_i - \frac{k_{T0,i}}{J_{0,i}R_{a0,i}}\tilde{d}_i + \dot{\omega}_{ref}) + \kappa_i \tilde{d}_i(-l_i \tilde{d}_i + \dot{d}_i) \leq -\frac{\omega_{sc}}{2}\tilde{\omega}_i^2 - (\kappa_i l_i - \frac{k_{T0,i}^2}{2\omega_{sc} J_{0,i}^2 R_{a0,i}^2})\tilde{d}_i^2 + \dot{\omega}_{ref}\tilde{\omega}_i + \kappa_i \dot{d}_i \tilde{d}_i$, $\forall t \geq 0$, where Lemma 1 and Young's inequality of $xy \leq \frac{\epsilon}{2}x^2 + \frac{1}{2\epsilon}y^2$, $\forall \epsilon > 0$, justify the inequality. The constant of $\kappa_i := \frac{1}{l_i}(\frac{k_{T0,i}^2}{2\omega_{sc} J_{0,i}^2 R_{a0,i}^2} + \frac{1}{2})$ finds an upper bound of $\dot{V}_i$ as $\dot{V}_i \leq -\alpha V_i + \dot{\omega}_{ref}\tilde{\omega}_i + \kappa_i \dot{d}_i \tilde{d}_i$, $\forall t \geq 0$, with $\alpha := \min\{\omega_{sc}, \frac{1}{\kappa_i}\}$, which shows the strict passivity of $\begin{bmatrix} \dot{\omega}_{ref} & \kappa_i \dot{d}_i \end{bmatrix}^T \mapsto \begin{bmatrix} \tilde{\omega}_i & \tilde{d}_i \end{bmatrix}$ that is equivalent to $\mathcal{L}_2$-stability for the same input-output mapping [25]. Therefore, it holds that $\tilde{\omega}_i \to 0$ and $\tilde{d}_i \to 0$ as $\dot{\omega}_{ref} \to 0$ and $\dot{d}_i \to 0$, exponentially. ■

Before proving the tracking performance recovery property, define the target tracking performance as

$$\dot{\omega}_i^* = \hat{\omega}_{sc}(\omega_{ref} - \omega_i^*), \ i = 1, \cdots, N, \ \forall t \geq 0, \quad (14)$$

which can be interpreted as a first-order time-varying low-pass filter (LPF). Theorem 2 asserts the speed tracking performance recovery property with respect to (14).

Theorem 2: The proposed control scheme of (7) with auto-tuning synchronizer of (8) and DOB of (9)-(10) guarantees that $\lim_{t\to\infty} |\omega_i(t) - \omega_i^*(t)| = 0$ as $\dot{d}_i(t) \to 0$, exponentially. $\diamondsuit$

Proof: Defining the error of $\tilde{\omega}_i^* := \omega_i^* - \omega_i$, it holds that

$$\dot{\tilde{\omega}}_i^* = \dot{\omega}_i^* - \dot{\omega}_i = -\hat{\omega}_{sc}\tilde{\omega}_i^* - \frac{k_{T0,i}}{J_{0,i}R_{a0,i}}\tilde{d}_i, \quad (15)$$

$i = 1, \cdots, N$, $\forall t \geq 0$. Consider the positive-definite function of $V_i^* := \frac{1}{2}\tilde{\omega}_i^* + \frac{b_i}{2}\tilde{d}_i$, $i = 1, \cdots, N$, $\forall t \geq 0$, which gives (using (12) and (15)) : $\dot{V}_i^* = \tilde{\omega}_i^*(-\hat{\omega}_{sc}\tilde{\omega}_i^* - \frac{k_{T0,i}}{J_{0,i}R_{a0,i}}\tilde{d}_i) + b_i\tilde{d}_i(-l_i\tilde{d}_i + \dot{d}_i) \leq -\frac{\omega_{sc}}{2}(\tilde{\omega}_i^*)^2 - (b_i l_i - \frac{k_{T0,i}^2}{2\omega_{sc} J_{0,i}^2 R_{a0,i}^2})\tilde{d}_i^2 + b_i \dot{d}_i \tilde{d}_i$, $\forall t \geq 0$, where the inequality is obtained by Lemma 1 and Young's inequality. The constant of $b_i := \frac{1}{l_i}(\frac{k_{T0,i}^2}{2\omega_{sc} J_{0,i}^2 R_{a0,i}^2} + \frac{1}{2})$ establishes an upper bound of $\dot{V}_i^*$ as $\dot{V}_i^* \leq -\beta V_i^* - b_i \dot{d}_i \tilde{d}_i$, $i = 1, \cdots, N$, $\forall t \geq 0$, with $\beta := \min\{\omega_{sc}, \frac{1}{b_i}\}$, which shows that $\tilde{\omega}^* \to 0$ as $\dot{d}_i \to 0$, exponentially. The proof is completed. ■

From Theorem 2, the closed-loop system driven by the proposed controller always ensures a better tracking performance than the originally desired performance of (5) since the target system of (14) magnifies the cut-off frequency from its initial value thanks to the auto-tuning synchronizer, i.e., $\hat{\omega}_{sc} \geq \omega_{sc}$, $\forall t \geq 0$ (see Lemma 1).

Before showing the speed synchronization property, consider the synchronization error dynamics as

$$\Delta\dot{\omega}_i = -\hat{\omega}_{sc}\Delta\omega_i + \frac{k_{T0,i}}{J_{0,i}R_{a0,i}}\tilde{d}_i - \frac{k_{T0,i+1}}{J_{0,i+1}R_{a0,i+1}}\tilde{d}_{i+1}, \quad (16)$$

$i = 1, \cdots, N$, $\forall t \geq 0$, which acts as the basis for the synchronization property analysis in Theorem 3.

Theorem 3: The proposed control scheme of (7) with auto-tuning synchronizer of (8) and DOB of (9)-(10) guarantees that $\lim_{t\to\infty} |\omega_i(t) - \omega_{i+1}(t)| = 0$, $i = 1, \cdots, N-1$ as $\dot{d}_i(t) \to 0$, $i = 1, \cdots, N$, exponentially. $\diamondsuit$

Proof: Consider the positive-definite function:

$$V_{sync} := \frac{1}{2}\sum_{i=1}^{N-1}\Delta\omega_i^2 + \sum_{i=1}^{N}\frac{c_i}{2}\tilde{d}_i^2 + \frac{1}{2\gamma_{at}}\tilde{\omega}_{sc}^2, \quad (17)$$

$c_i > 0$, $\forall t \geq 0$. The closed-loop trajectories of (8), (12), and (16), renders $\dot{V}_{sync}$ to be : $\dot{V}_{sync} = -\omega_{sc}\sum_{i=1}^{N-1}\Delta\omega_i^2 + \sum_{i=1}^{N-1}\Delta\omega_i(\frac{k_{T0,i}}{J_{0,i}R_{a0,i}}\tilde{d}_i - \frac{k_{T0,i+1}}{J_{0,i+1}R_{a0,i+1}}\tilde{d}_{i+1}) - \sum_{i=1}^{N} c_i l_i \tilde{d}_i^2 + \sum_{i=1}^{N} c_i \dot{d}_i \tilde{d}_i - \rho_{at}\tilde{\omega}_{sc}^2 \leq -\frac{\omega_{sc}}{3}\sum_{i=1}^{N-1}\Delta\omega_i^2 - \sum_{i=1}^{N}(c_i l_i - \zeta_i)\tilde{d}_i^2 - \rho_{at}\tilde{\omega}_{sc}^2 + \sum_{i=1}^{N} c_i \dot{d}_i \tilde{d}_i$, $\forall t \geq 0$, where the inequality is obtained by Young's inequality for some constant of $\zeta_i > 0$. The constant of $c_i := \frac{1}{l_i}(\zeta_i + \frac{1}{2})$ results in an upper bound for the inequality of $\dot{V}_{sync}$ as $\dot{V}_{sync} \leq -\sigma V_{sync} + \sum_{i=1}^{N} c_i \dot{d}_i \tilde{d}_i$, $\forall t \geq 0$, with $\sigma := \min\{\frac{2\omega_{sc}}{3}, \frac{1}{c_1}, \cdots, \frac{1}{c_n}, 2\rho_{at}\gamma_{at}\}$. This shows that $\Delta\omega_i \to 0$ as $\dot{d}_i \to 0$. The proof is completed. ■

Define the target synchronization performance as

$$\Delta\dot{\omega}_i^* = -\hat{\omega}_{sc}\Delta\omega_i^*, \ i = 1, \cdots, N-1, \ \forall t \geq 0, \quad (18)$$

which is used to assert the synchronization performance recovery property with respect to (18) in Theorem 4

Theorem 4: The proposed control scheme of (7) with auto-tuning synchronizer of (8) and DOB of (9)-(10) guarantees that $\lim_{t\to\infty} |\Delta\omega_i(t) - \Delta\omega_i^*(t)| = 0$, $i = 1, \cdots, N-1$ as $\dot{d}_i(t) \to 0$, $i = 1, \cdots, N$, exponentially. $\diamondsuit$

Proof: The error, defined as $\Delta\tilde{\omega}_i^* := \Delta\omega_i^* - \Delta\omega_i$, yields:

$$\Delta\dot{\tilde{\omega}}_i^* = -\hat{\omega}_{sc}\Delta\tilde{\omega}_i^* - \frac{k_{T0,i}}{J_{0,i}R_{a0,i}}\tilde{d}_i + \frac{k_{T0,i+1}}{J_{0,i+1}R_{a0,i+1}}\tilde{d}_{i+1}, \quad (19)$$

$i = 1, \cdots, N-1$, $\forall t \geq 0$. Consider the positive-definite function using (17) as $V_{sync}^* := V_{sync}\Big|_{\Delta\omega_i = \Delta\tilde{\omega}_i^*}$, $\forall t \geq 0$. Then, since the trajectories of (16) and (19) have the same form, $\dot{V}_{sync}^*$ can be easily obtained as $\dot{V}_{sync}^* \leq -\sigma V_{sync}^* + \sum_{i=1}^{N} c_i \dot{d}_i \tilde{d}_i$, $\forall t \geq 0$, in the same manner as the proof of Theorem 3. This completes the proof. ■

From the result of Theorem 4, the closed-loop system driven by the proposed controller always ensures a better synchronization performance than the originally desired performance of (5) since the target system of (14) magnifies the cut-off frequency from its initial value thanks to the auto-tuner, i.e., $\hat{\omega}_{sc} \geq \omega_{sc}$, $\forall t \geq 0$ (see Lemma 1).

This article has been accepted for publication in a future issue of this journal, but has not been fully edited. Content may change prior to final publication. Citation information: DOI 10.1109/TCSII.2019.2915384, IEEE Transactions on Circuits and Systems II: Express Briefs

The absence of integral action in the control law leads to concern about steady-state error in actual implementations, which is addressed in Theorem 5.

Theorem 5: The proposed control scheme of (7) with auto-tuning synchronizer of (8) and DOB of (9)-(10) guarantees the offset-free property for the both tracking and synchronization. i.e., $\omega_{i,\infty} = \omega_{ref,\infty}, \omega_{i,\infty} = \omega_{i+1,\infty}$, $i = 1, \cdots, N$, where $\lim_{t\to\infty} f = f_\infty$ for any convergent function of f. ◇

Proof: The closed-loop steady-state equations can be obtained from (11), (12), and (16) as $0 = \hat{\omega}_{sc,\infty}\tilde{\omega}_{i,\infty} + \frac{k_{T0,i}}{J_{0,i}R_{a0,i}}\tilde{d}_{i,\infty}$, $0 = l_i\tilde{d}_{i,\infty}$, and $0 = \hat{\omega}_{sc,\infty}\Delta\omega_{i,\infty} - \frac{k_{T0,i}}{J_{0,i}R_{a0,i}}\tilde{d}_{i,\infty} + \frac{k_{T0,i+1}}{J_{0,i+1}R_{a0,i+1}}\tilde{d}_{i+1\infty}$. The combination of these equations confirms that the Theorem 5 holds true. ■

IV. Experimental Results

This section experimentally shows the effectiveness of the proposed scheme, by using a two-motor system, and comparing it with a conventional relative cross-coupling controller and adaptive synchronizer. A 50W prototype DC motor and driver were used with a DC-Link voltage level of $V_{dc} = 12$V. The control algorithms were implemented with a National Instrument (NI) MyRIO-1900 in the math-script provided in LabVIEW software. The sampling/control period was set to 10 ms. Fig. 2 shows the hardware implementation.

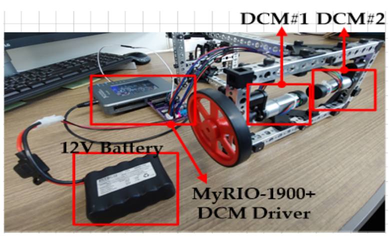

Fig. 2. Experimental setup

The DC motor parameters were identified as $R_a = 3.3\ \Omega$, $L_a = 1.16\ mH$, $k_T = k_e = 0.373\ V/rad/s$, $J = 9.85 \times 10^{-5}\ kg \cdot m^2$, $B = 9.85 \times 10^{-6}\ N_m/rad/s$, and the nominal DC motor parameters used for the controller were selected as $J_{0,i} = 0.6J$, $k_{T0,i} = 1.4k_T$, $R_{a0,i} = 0.8R_a$, $i = 1, 2$. The initial speed cut-off frequency was set to $f_{sc} = 0.2$ Hz for $\omega_{sc} = 2\pi f_{sc} = 1.256$ rad/s. The remaining design parameters were tuned as $l_i = 62.8$, $\gamma_{at} = 2$, and $\rho_{at} = 1/\gamma_{at}$.

A. Effectiveness of Proposed Synchronizer

The goal of the first experiment is to verify the efficacy of the proposed synchronizer. To this end, while running at a speed of 2000 rpm, a synchronization error was induced by applying an abrupt load torque to the wheel attached to the first motor. Fig. 3 shows the resulting synchronization error behaviors while turning the synchronizer ON and OFF. The corresponding cut-off frequency and estimated disturbance signals are given in Fig. 4. From this result, it can bee seen that the proposed controller accomplishes a considerable reduction of the synchronization error in transient periods without any overshoots.

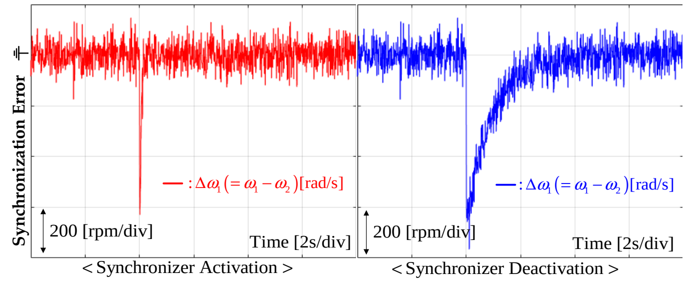

Fig. 3. Speed synchronization error behavior comparison with and without proposed synchronizer

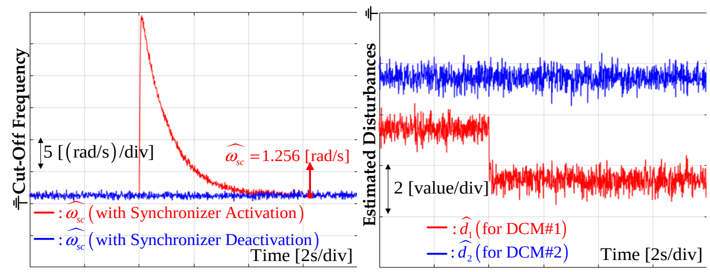

Fig. 4. Cut-off frequency and DOB responses

B. Comparison with Relative Cross-Coupling

Another recent synchronization control technique was considered for comparison. The approach consists of a PI controller equipped with relative cross-coupling and active-damping compensation terms: $v_{a,i} = -B_{d,i}\omega_i + \frac{J_{0,i}R_{a0,i}}{k_{T0,i}}\omega_{sc}\tilde{\omega}_i + B_{d,i}\omega_{sc}\int_0^t \tilde{\omega}_i(\tau)d\tau + (-1)^i k_i\Delta\omega_1$, $i = 1, 2$, $\forall t \geq 0$, with active-damping and cross-coupling gains of $B_d > 0$ and $k_i > 0$, $i = 1, 2$. These terms were set to $B_d = 0.1$, and $k_i = 0.1$, $i = 1, 2$ to achieve acceptable closed-loop performance. It is easy to see that this controller makes the closed-loop dynamics to be (5) in the absence of cross-coupling terms and parameter uncertainties, i.e., $J_{0,i} = J_i$, $k_{T0,i} = k_{T,i}$, $R_{a0,i} = R_{a,i}$, $i = 1, 2$.

The experimental scenario was the same as in the first experiment. Fig. 5 presents the synchronization error behavior comparison. As can be seen from these results, the proposed synchronizer more effectively eliminates synchronization error compared to the cross-coupling compensation-based controller.

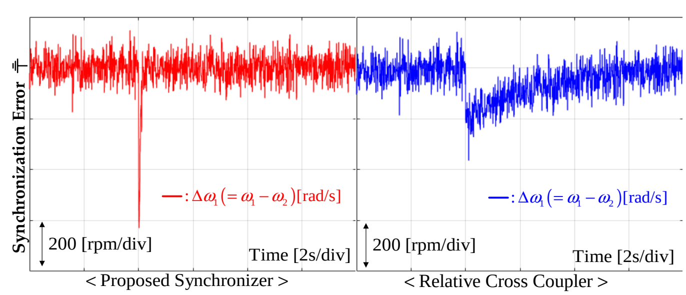

Fig. 5. Speed synchronization error behavior comparison with cross-coupling compensation-based controller

This article has been accepted for publication in a future issue of this journal, but has not been fully edited. Content may change prior to final publication. Citation information: DOI 10.1109/TCSII.2019.2915384, IEEE Transactions on Circuits and Systems II: Express Briefs

C. Comparison with Adaptive Synchronizer

This section experimentally compares the synchronization performance with a recent adaptive synchronizer by replacing the proposed synchronizer of (8) with

$$\dot{\hat{\omega}}_{sc} = \gamma_{at} \Delta\omega_1^2, \ \forall t \geq 0, \tag{20}$$

which was introduced as the auto-tuner for PID gains in [26]. The design parameter of γ_{at} was set to the same value as the proposed synchronizer. Fig. 6 depicts the comparison result. There was no difference between the speed synchronization performances, but the adaptive synchronizer fails to stabilize to its initial value. Note that keeping the magnified cut-off frequency, used for the feedback gain, could result in a closed-loop efficiency degradation, or even instability.

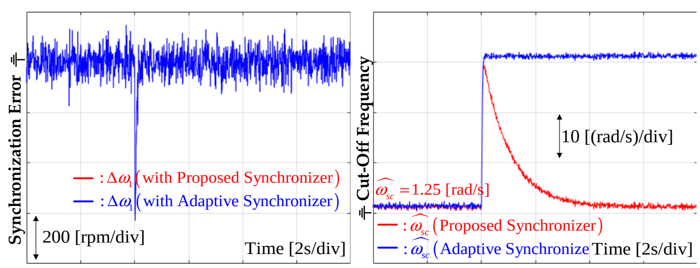

Fig. 6. Speed synchronization error and cut-off frequency behavior comparison with adaptive synchronizer

From these experimental results show that the useful properties derived in Section III-B do, indeed, contribute to a considerable reduction of synchronization error.

V. Conclusions

The proposed proportional-type DC motor synchronization scheme was designed to guarantee attractive closed-loop properties, performance recovery without steady state errors. The practical constraints of parameter and load variations were systematically handled in the controller design procedure. The experimental data confirmed the advantages coming from the closed-loop properties under a load torque variation scenario. As a future research direction, this result will be applied to three-phase motor control systems, such as those implemented for induction and permanent magnet synchronous machines.

References

[1] Xian Hui Mai, Du Qu Wei, Bo Zhang, and Xiao Shu Luo. Controlling chaos in complex motor networks by environment. *IEEE Trans. Circuits Syst. II Express Briefs*, 62:603–607, 2015.

[2] Suman Ghosh, Mousam Ghosh, Goutam Kumar Panda, and Pradip Kumar Saha. Mechanical contact-less computational speed sensing approach of PWM operated PMDC brushed motor: A slotting-effect and commutation phenomenon incorporated semi-analytical dynamic model-based approach. *IEEE Trans. Circuits Syst. II Express Briefs*, 65:81–85, 2018.

[3] Dongdong Wang, Bo Zhang, Dongyuan Qiu, Fan Xie, and Duqu Wei. Stability analysis of the coupled synchronous reluctance motor drives. *IEEE Trans. Circuits Syst. II Express Briefs*, 64:196–200, 2017.

[4] Araz Darba, Frederik De Belie, Pieter D'haese, and Jan A. Melkebeek. Improved dynamic behavior in BLDC drives using model predictive speed and current control. *IEEE Trans. Ind. Electron.*, 63:728–740, 2016.

[5] A. Rubaai and R. Kotaru. Online identification and control of a DC motor using learning adaptation of neural networks. *IEEE Trans. Ind. Appl.*, 36:935–942, 2000.

[6] S.-K. Sul. *Control of Electric Machine Drive Systems, Vol.88*. Hoboken, NJ, USA: Wiley, 2011.

[7] G.-D. Andeescu, C.Pitic, F. Blaabjerg, and I. Boldea. Combined flux observer with signal injection enhancement for wide speed range sensorless direct torque control of IPMSM drives. *IEEE Trans. on Energy Convers.*, 23:393–402, 2008.

[8] L. Tang, L. Zhong, M. Rahman, and Y. Hu. A novel direct torque control for interior permanent-magnet synchronous machine drive with low ripple in torque and flux - a speed-senseroless approach. *IEEE Trans. on Ind. Appl.*, 39:1748–1756, 2003.

[9] Haitao Yang, Yongchang Zhang, Jiejunyi Liang, Bo Xia, Paul D. Walker, and Nong Zhang. Deadbeat control based on a multipurpose disturbance observer for permanent magnet synchronous motors. *IET Electric Power Appl.*, 12:708–716, 2018.

[10] Xudong Liu, Haisheng Yu, Jinpeng Yu, and Lin Zhao. Combined speed and current terminal sliding mode control with nonlinear disturbance observer for PMSM drive. *IEEE Access*, 6:29594–29601, 2018.

[11] Jesus Linares-Flores, Carlos Garcia-Rodriguez, Hebertt Sira-Ramirez, and Oscar David Ramirez-Cardenas. Robust backstepping tracking controller for low-speed PMSM positioning system: Design, analysis, and implementation. *IEEE Trans. Ind. Inf.*, 11:1130–1141, 2015.

[12] R. Errouissi, M. Ouhrouche, W.-Hua Chen, and A. M. Trzynadlowski. Robust cascaded nonlinear predictive control of a permanent magnet synchronous motor with antiwindup compensator. *IEEE Trans. Ind. Electron.*, 59:3078–3088, 2012.

[13] M. L. Corradini, G. Ippoliti, S. Longhi, and G. Orlando. A quasi-sliding mode approach for robust control and speed estimation of PM synchronous motors. *IEEE Trans. Ind. Electron.*, 59:1096–1104, 2012.

[14] G. Papafotieu, J. Kley, K. Papdopoulous, P. Bohren, and M. Morari. Model predictive direct torque control-part II: implementation and experimental evaluation. *IEEE Trans. Ind. Electron.*, 56:1906–1915, 2009.

[15] S.-K. Kim, K.-G. Lee, and K.-B. Lee. Singularity-free adaptive speed tracking control for uncertain permanent magnet synchronous motor. *IEEE Trans. Power Electron.*, 31:1692–1701, 2016.

[16] S.-K. Kim, J.-S. Lee, and K.-B. Lee. Offset-free robust adaptive backstepping speed control for uncertain permanent magnet synchronous motor. *IEEE Trans. Power Electron.*, 10:7065–7076, 2016.

[17] S.-K. Kim, J.-S. Lee, and K.-B. Lee. Self-tuning adaptive speed controller for permanent magnet synchronous motor. *IEEE Trans. Power Electron.*, 32:1493–1506, 2017.

[18] S.-K. Kim. Robust adaptive speed regulator with self-tuning law for surfaced-mounted permanent magnet synchronous motor. *Control Eng. Pract.*, 61:55–71, 2017.

[19] Young Ik Son, In Hyuk Kim, Dae Sik Choi, and Hyungbo Shim. Robust cascade control of electric motor drives using dual reduced-order PI observer. *IEEE Trans. Ind. Electron.*, 62:3672–3682, 2015.

[20] D. Z. Zhao, C. W. Li, and J. Ren. Speed synchronisation of multiple induction motors with adjacent cross-coupling control. *IET Control Theory and Appl.*, 4:119–128, 2008.

[21] Shuyi Lin, Yunze Cai, Bo Yang, and Weidong Zhang. Electrical line-shafting control for motor speed synchronisation using sliding mode controller and disturbance observer. *IET Control Theory and Appl.*, 11:205–212, 2016.

[22] Y. T. Shih, C. S. Chen, and A. C. Lee. A novel cross-coupling control design for bi-axis motion. *Int. J. Mach. Tools Manuf.*, 42:1539–1548, 2002.

[23] Y. Xiao and K. Y. Zhu. A cross-coupling reference model control algorithm. *Int. J. Adapt. Control Signal Process.*, 19:623–638, 2005.

[24] Y. Xiao and K. Y. Zhu. Optimal synchronization control of high-precision motion systems. *IEEE Trans. Ind. Electron.*, 53:1160–1169, 2006.

[25] Hassan K. Khalil. *Nonlinear Systems*. Prentice Hall, 2002.

[26] Jin-Woo Jung, Viet Quoc Leu, Ton Duc Do, Eun-Kyung Kim, and Han Ho Choi. Adaptive PID speed control design for permanent magnet synchronous motor drives. *IEEE Trans. Power Electron.*, 30:900–908, 2015.